



Solar radiation transmission through conifer canopies

J.P. Hardy^{a,*}, R. Melloh^a, G. Koenig^a, D. Marks^b, A. Winstral^b,
J.W. Pomeroy^c, T. Link^d

^aCold Regions Research and Engineering Laboratory, US Army Engineering Research Development Center, Hanover, NH 03755, USA

^bUSDA-Agricultural Research Station, Boise, ID, USA

^cUniversity of Saskatchewan, Saskatoon, Sask., Canada

^dUniversity of Idaho, Moscow, ID, USA

Received 9 February 2004; accepted 25 June 2004

Abstract

Energy budget dynamics under forest canopies are strongly influenced by the large spatial variability of radiative and turbulent transfers in this environment. Incoming solar radiation under canopies has a particularly high degree of spatial variability. Transmission of solar radiation through a forest canopy varies with the size and location of the canopy gaps, as well as canopy leaf area. Modeling this transmission has proven challenging owing to the highly variable nature of the gaps within and between tree crowns, particularly in discontinuous canopies. This study describes and simulates the solar variability incident on the snow surface beneath two conifer forests.

Objectives of this work are (1) to evaluate the variability of incoming solar radiation data with respect to canopy structure and cloudiness, (2) to correlate measured solar radiation transmission with predicted solar transmission based on analysis of hemispherical photographs, and (3) to examine the impact of measured and predicted transmission factors on the seasonal net radiative exchanges and snow ablation, based on snow process modeling. Observations were made during the winters of 2002 and 2003 in two predominately lodgepole pine (*Pinus contorta*) stands, one discontinuous and one relatively uniform, at the Local Scale Observation Site (LSOS) in Fraser, CO, USA, as part of the Cold Land Processes Experiment (CLPX). The canopy structure of all trees in the 0.8 ha triangular plot was measured and mapped in detail. We measured incoming global solar radiation at the snow surface beneath the discontinuous and the uniform canopies using arrays of 10 upward looking pyranometers at each site. Incoming global solar radiation was also measured above the canopy. Hemispherical photographs were taken with a Nikon Coolpix 995 with a fisheye converter at each radiometer location in both canopies, and were analyzed with Gap Light Analyzer (GLA) software. We found good agreement between measured and GLA-predicted transmissivities ($r^2 = 0.86$) when all data from both years were considered. Transmission factors derived from hemispheric photos and GLA software can be used to specify the distribution of solar flux under a canopy, instead of direct solar flux measurements, without degradation in snow model melt predictions.

© 2004 Elsevier B.V. All rights reserved.

Keywords: Transmissivity of canopy to direct radiation; Hemispherical photography; Canopy light gaps; Solar radiation; Snowcover

* Corresponding author. Tel.: +1 603 646 4360; fax: +1 603 646 4397.

E-mail address: janet.p.hardy@erdc.usace.army.mil (J.P. Hardy).

1. Introduction

Accurate characterization of the radiation regime beneath a forest canopy is important for validation of physically based canopy models, assessment of variability of both solar and longwave radiative components, and input to energy-balance models concerned with the snow cover or soil conditions beneath a canopy. The forest canopy architecture (tree elements and gaps) strongly influences solar radiation interception and transmittance and varies with space and time, and depends on tree species, size and location of canopy gaps, and on the angle of solar incidence. Energy balance modeling at the stand scale presents challenges to account for these large variations of solar radiation incident on the forest floor.

Radiative transfer through a forest canopy is complex and is treated differently in energy transfer models. Transmissivity is the dimensionless ratio of radiation transmitted through the canopy to that incident upon it. A Beer's-type law approach is used to describe the probability of a photon reaching the ground beneath a horizontal, homogeneous canopy layer. Many modelers use a variation on the general Beer's law equation (Eq. (1)) to attenuate incident solar radiation to the understory (Wigmosta et al., 1994; Nijssen and Lettenmaier, 1999; Link and Marks, 1999; Hellstrom, 2000)

$$K \downarrow_{\text{sub-canopy}} = K \downarrow_{\text{above}} e^{-f} \quad (1)$$

where $K \downarrow$ is the incoming solar radiation either above or below the canopy, and f is the bulk canopy optical thickness, which depends on leaf area index (LAI) and other variables (canopy structure, solar zenith and azimuth angles). Models differ in how they prescribe f . Tarboton and Luce (1996) used linear relationships to reduce net radiation fluxes in their UEBFC snow model Eq. (2),

$$K^* = (1 - \text{FC})K \downarrow_{\text{above}}(1 - \alpha_s) \quad (2)$$

where K^* is the net solar radiation below the canopy, FC is the forest canopy closure, and α_s is the snow surface albedo. Hellstrom (2000) later modified the Tarboton and Luce (1996) algorithm and incorporated a variation of Beer's law (Beer–Lambert), which assumes random distribution of leaves and branches. Pomeroy and Dion (1996) also used a Beer's law

variant to describe the transmission of light through the forest needles, branches, and intercepted snow. These Beer's law variants fail to describe the light passing through the more realistic, discontinuous canopy structure, where gaps are non-uniform and light is scattered by the canopy elements. The geometric-optical radiative-transfer (GORT) model developed by Li et al. (1995) is a complex model that considers the three-dimensional geometry of forest canopy and includes multiple scattering within and between crowns. While the model has proven effective and has successfully predicted radiation transfer through randomly distributed canopies (Ni et al., 1997; Hardy et al., 1997, 1998), it requires many parameters that are difficult to measure in the field (i.e., crown geometry, foliage area volume density). Roujean (1999) also describes a two-dimensional model (TSETSE) for transmitted radiation beneath conifer stands. This local-scale model contains a geometric component to describe the between-crown gap probability and a volume component to simulate the radiative transfer within a single crown. The model is written as a product of factors of interception rather than transmission.

Accurate characterization and modeling of the sub-canopy solar radiation regime is required to adequately describe the exchanges in fluxes of energy and mass, as well as for remote sensing. Measurement of solar variability beneath canopies is difficult owing to the extreme variability of these fluxes and the expense of multiple sensors (Link et al., in press). Arrays of 10 or more radiometers have successfully described the radiation regimes within forest canopies (Hardy et al., 1997, 1998; Link and Marks, 1999; Tribbeck, 2002; Melloh et al., 2002). Hardy et al. (2001) used previously measured solar transmissivities in a deciduous boreal forest (Hardy et al., 1998) to estimate transmissivity through a deciduous forest in New Hampshire, where the canopy structure was known, but array data unavailable. The purpose of that work was to estimate solar fluxes reaching the snow surface beneath the canopy for snow modeling. Their results suggest some transferability of measured transmissivity among similar forest types (structure, species). Rowlands et al. (2002) considered the variability of sub-canopy solar and longwave radiation as a function of cloudiness and temporal averaging in discontinuous and uniform canopies. Both canopies

displayed high variability in incoming solar radiation during clear and cloudy days, for short time intervals of 1–5 min (coefficient of variation (CV), ~ 1.0 for clear days, and ~ 0.5 for cloudy days). For longer time intervals (daily averages) the CV decreased to 0.09 on clear days and to 0.08 on cloudy days in the uniform canopy, and 0.26 (clear days) to 0.29 (cloudy days) in the discontinuous canopy. The persistence of high variability in the discontinuous canopy suggests that consideration of the spatial variability of insolation in these canopies is a priority for accurately modeling snowmelt processes.

Hemispherical (fisheye) photography is a technique for characterizing plant canopies using upward looking photographs taken through an extremely wide-angle lens (Rich, 1990; Gendron et al., 1998). Typically, the viewing angle approaches or equals 180° . The resulting photographs serve as semi-permanent records of the geometry of canopy openings and are used in studies of forest canopy dynamics to derive such parameters as LAI, gap fraction, and estimates of light indices (Whitford et al., 1995; Lin and Chiang, 2002). Evans and Coombe (1959) estimated sunlight penetration through forest canopy openings by overlaying diagrams of the sun track on hemispherical photographs. Later, Anderson (1964) provided a thorough theoretical treatment for calculating the penetration of direct and diffuse components of solar radiation through canopy openings as determined using hemispherical photographs. The distribution of canopy gaps can be measured precisely and used to estimate potential solar radiation penetration (Rich, 1990; Hellstrom, 2000; Chen et al., 1991; Canham, 1995). Nakabayashi et al. (1999) used hemispherical photographs to determine total, and sun path, sky view factors to improve estimates of net radiation in a forested basin in Japan, to better predict the quantity and timing of snowmelt. Hellstrom (2000) used fisheye photography to calculate a hemispherical sky view factor, which represents the weighted gap fraction at the forest floor by accounting for the angle of incidence on a horizontal plane and for the variations of canopy cover.

The objectives of this work are (1) to evaluate the variability of incoming solar radiation data with respect to canopy structure and cloudiness, (2) to correlate measured solar radiation transmission with

predicted solar transmission based on analysis of hemispherical photographs, and (3) to examine the impact of measured and predicted transmission factors on the seasonal net radiative exchanges and snow ablation, based on snow process modeling. Additionally, we will determine if predicted transmission factors can be used instead of measurements to derive the solar fluxes under canopies in discontinuous forested areas. If so, then the advantage to this inexpensive approach is that the transmission factors are easily obtained from hemispheric photos and, when combined with incident solar flux data above the canopy, allow distribution of flux beneath the canopies.

2. Methods

2.1. Site description and field measurements

During the winters of 2002 and 2003, we made observations in two predominately lodgepole pine (*Pinus contorta*) stands, one beneath a discontinuous canopy and the other beneath a uniform canopy, at the local scale observation site (LSOS) in the US Forest Service, Fraser Experimental Forest in Fraser, Colorado, USA (39.9°N ; 105.9°W ; 2780 m asl). This work was part of the larger, multi-institution effort, Cold Land Processes Experiment (CLPX) (Cline et al., 2002). The CLPX measurements consisted of four 6-day intensive observation periods: 19–24 February and 24–30 March during both winters. The 0.8 ha triangular LSOS consisted of a small clearing, a managed uniform pine canopy, and a discontinuous, mixed age canopy (Fig. 1). We defined and extensively mapped the canopy in the LSOS. The area was divided into 78 plots, each $10\text{ m} \times 10\text{ m}$, and in 62 of the plots, the individual tree locations were mapped and linked to measurements of their structure (tree height, crown height, diameter at breast height, and crown diameter). The uniform pine site consists of lodgepole pine trees with an average height of 12.4 m (standard deviation = 2.5 m; $n = 88$) and relatively uniform spacing between trees. Trees in the discontinuous site are of mixed species [predominantly lodgepole pine with some Engelmann Spruce (*Picea engelmannii*) and Subalpine Fir (*Abies lasiocarpa*)] with an average tree height of

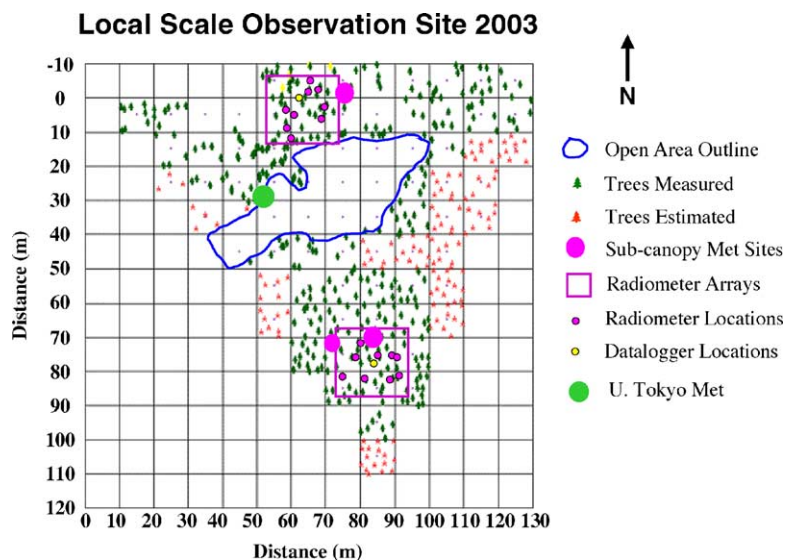


Fig. 1. LSOS showing radiometer locations for 2003. The uniform pine stand is south and east of the open clearing. The discontinuous pine site is located north and west of the clearing.

7.8 m (standard deviation = 4.8 m; $n = 88$) and heterogeneous spacing between trees.

2.2. Local meteorological and snow property measurements

As part of the CLPX and on-going measurements at the Fraser Experimental Forest, a meteorological tower was erected in a small clearing near the LSOS. Data collection is ongoing since February 2002. Standard meteorological data (air temperature, relative humidity, wind speed) were measured at this site at several heights and stored on a Campbell Scientific datalogger. Additionally, incoming global solar radiation and incoming longwave radiation were measured at the top of the tower at heights greater than the surrounding trees. Precipitation (water equivalent) and snow depth were continuously monitored. During the experiment's observation periods, we measured detailed snow properties (depth, density, grain size and shape, temperature, and stratigraphy) at three sites each day at the LSOS. Available data were used for initializing the snow model, SNOBAL, and as forcing data for running the model from mid-winter through snowmelt.

2.3. Sub-canopy solar irradiance measurements

We measured incoming global solar radiation at the snow surface beneath the discontinuous and the uniform pine canopies during the four observation periods, using arrays of 10 upward looking pyranometers. Pyranometer locations within each canopy type were different for each of the 2 years, allowing for 40 unique radiometer locations. The arrays consisted of Eppley Precision Spectral Pyranometers (PSP, 0.3–3.0 μm wavelength, 160° sky view, 5% accuracy), placed on the snow surface in the forest stand, and were used to measure variability of solar irradiance beneath the canopy (Link et al., in press). We programmed the Campbell Scientific CR10 datalogger to measure irradiance every 10 s and output 5 min averages. Pyranometers were labeled PSP1 through PSP10. The locations of the pyranometers represented the variability of solar receipt in that some were placed adjacent to a tree stem in different cardinal directions, while others were located beneath small canopy gaps. Each pyranometer sat on a small piece of 0.06 m-thick foam to provide stability on the snow surface; the instrument level was checked daily. Every morning, and throughout the day, as necessary, all pyranometers were cleared of any accumulated snow or frost, and the

time of clearing noted. Measured solar transmittance through the canopy was determined according to Eq. (3), where τ_c is the canopy transmittance and $K\downarrow$ is the measured incoming solar radiation

$$\tau_c = \frac{K\downarrow_{\text{sub-canopy}}}{K\downarrow_{\text{above}}} \quad (3)$$

2.4. Hemispherical photography and analysis software

Hemispherical photos were taken approximately 1 m above each of the 40 different radiometer locations in both canopies using a Nikon Coolpix 995 digital camera equipped with a Nikon Fisheye Converter (FC-E8). The camera and lens provided a focal length equivalent to 7.2 mm, and a combined f -number of $f/2.6$, with a full 183° field-of-view. The camera was mounted on a tripod, leveled horizontally using a bubble level, and oriented such that north corresponded to the top of the photograph (Fig. 2). We took the images on an overcast day to provide uniform lighting and illumination of the canopy. Images were saved in JPEG format and according to Frazer et al.



Fig. 2. Hemispherical camera and tripod set up in the discontinuous forest site. The plastic bag was removed prior to obtaining imagery.

(2001), the image compromise attributable to compression was negligible. More information concerning the performance of this camera and lens setup for hemispherical photo analysis was presented in Frazer et al. (2001).

We used the scientific image processing software, Gap Light Analyzer (GLA) Version 2.0 developed by Frazer et al. (1999, 2000), to process and analyze the digital hemispheric canopy images. The software extracts canopy structure data (gap fraction, canopy openness, effective LAI) and gap light transmission indices based on a user-specified day of interest. The simplified radiation model within GLA assumes that when the sun position is obstructed by the canopy, the direct radiation is zero, and when unobstructed, direct radiation is equal to the above-canopy value (Frazer et al., 1999). Beam enrichment by scattered and reflected radiation is not considered. Frazer et al. (1999) used the gap light index (GLI) developed by Canham (1988), which is in the form of Eq. (4),

$$\text{GLI} = [(T_{\text{diffuse}}P_{\text{diffuse}}) + (T_{\text{beam}}P_{\text{beam}})] \times 100 \quad (4)$$

where P_{diffuse} and P_{beam} are the proportions of incident radiation received at the top of the canopy as either diffuse sky radiation or direct beam radiation, respectively ($P_{\text{diffuse}} = 1 - P_{\text{beam}}$), and T_{diffuse} and T_{beam} are the proportions of diffuse and beam radiation that are transmitted through the gap to a point in the understory. The GLI ranges from 0, where theoretically there is no gap visible, to 100 for an open site and specifies the contribution of the gap to the light regime at the given point beneath the canopy. Comparisons of the GLI with long-term above and below canopy solar radiation data indicate a positive correlation ($r^2 > 0.93$; Canham, 1988; Gendron et al., 1998).

User-supplied input variables and our assumed values are summarized in Table 1. The following general description of these variables is from the GLA

Table 1
GLA user supplied variables

User supplied variables	Value
Cloudiness index	0.5
Spectral fraction (0.25–25 μm)	1
Beam fraction	0.5
Clear-sky transmission coefficient	0.7
Solar constant (assumed) (W m^{-2})	1367

Version 2.0 User Manual and Program Documentation. The cloudiness index is a site-specific measure of cloudiness and ranges from 0 to 1. The spectral fraction is the ratio of solar energy that falls within a limited range of the electromagnetic spectrum to the total shortwave radiation contributed by all wavelengths (0.25–25 μm). The beam fraction is the ratio of direct to global spectral radiation incident on a horizontal surface. The clear-sky transmission coefficient is a factor that describes the regional clarity of the atmosphere with respect to instantaneous transmission of direct radiation (approximately 0.3–3 μm) and ranges from 0.4 to 0.8. The solar constant is the total radiant flux of the sun outside the Earth's atmosphere.

Additional input variables include image orientation, site location, time step, sky regions, and dates of interest. We used the polar projection and divided the region into 10° intervals of zenith and azimuth angles (324 sky regions). The area of each image greater than an 80° zenith angle was masked to correspond with the 160° viewing geometry of the Eppley pyranometers. The maximum zenith angle of the mid-day sun path decreased from 53° to 39° between the February and March observation periods. For this reason, each hemispherical image was analyzed twice to account for the different configurations in the sun track as predicted by the GLA software (Fig. 3).

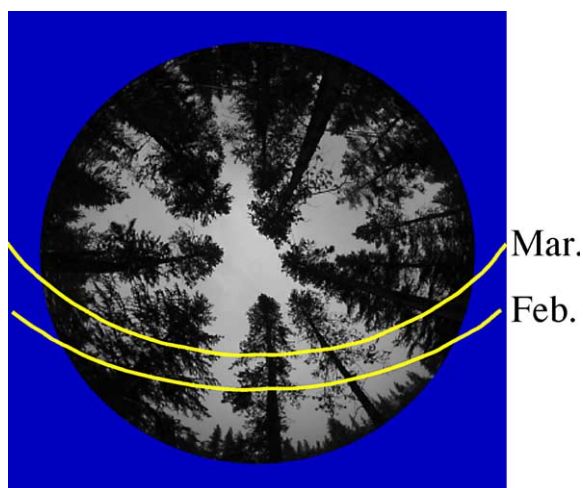


Fig. 3. Example of hemispherical photo showing suntrack positions for February and March and a 160° mask.

Table 2

Sensitivity test comparing GLA-predicted total solar transmissivities using different threshold values

Test for PSP4 (March 2003)	Threshold value	Percent total transmissivity
Measured	(135)	35.0
GLA, dark	170	27.4
GLA, light	80	49.2
GLA, initial	122	37.8
GLA, independent	128	36.7

The threshold value in parenthesis was necessary to obtain a transmissivity value equal to the measured transmissivity.

By designating an intensity threshold that best corresponded with the registered image, the software creates binary classes of sky (white) and canopy (black). This technique is subjective and introduces some chance for error owing to individual interpretation. For this reason, a sensitivity analysis was conducted for the discontinuous pine, PSP4, 2003 image (Table 2). This test evaluated the sensitivity of the software to varying threshold limits. The measured transmissivity at PSP4 was 35%, which required a threshold value of 135 to obtain a GLA-equivalent transmissivity. We tested the sensitivity of predicted transmission based on somewhat realistic high and low threshold values, and each affecting the predicted transmissivity by about 10%. Two experienced software users independently processed the image, resulting in an approximately 1% difference in transmissivity. Our initial processing of this image suggested a threshold value of 122, while an independent user chose a threshold value of 128, which was closer to the measured value and was adopted and used for processing all images.

2.5. Snow model

Snow energy balance modeling examined the influence of measured versus GLA-predicted transmissivities on net allwave radiation and snow depth. We used the SNOBAL model, which was first presented by Marks (1988) and later described by Marks et al. (1999) and runs using the Image Processing Workbench (IPW) (Frew, 1990). SNOBAL is an interactive point-scale model that uses the energy balance to calculate snowmelt from input data on snow properties and energy exchanges. The model approximates the

snow cover as two layers—a surface fixed-thickness active layer and a lower layer—solves for the temperature and mass per unit area for each layer, and computes the total snow cover. Input requirements include standard meteorological data (net solar radiation, incoming thermal radiation, air temperature, relative humidity, wind speed, soil temperature, and precipitation) as well as initialization data, such as snow properties (depth, density, temperature, water content). We ran SNOBAL twice, first by applying the mean measured transmissivity, and later the GLA-predicted transmissivity, to the above-canopy incoming solar radiation data. All other input parameters were held constant. We compared model predictions of snow depth and net allwave radiation beneath the uniform pine site using measured and GLA-predicted solar transmission factors.

3. Results and discussion

While sub-canopy radiation data were collected during four 6-day periods in both 2002 and 2003 beneath two forest canopies (uniform and discontinuous), our detailed analysis focused on the 2003 data from the discontinuous forest. The discontinuous pine site was selected because of the extreme variability of solar insolation resulting in a more complex forested environment. The combined 2002 and 2003 data from both sites were used to improve the statistical strength of the relationship between measured and modeled transmissivities. In general, the quality of the field data was excellent, as one person was dedicated to maintenance of the radiometers during the observation periods. For this analysis, we ignored data from days with constant precipitation owing to the difficulty in keeping the radiometer domes snow-free.

3.1. Radiometer array

Data from the radiometer array provided information on the nature and variability of sub-canopy insolation in the uniform and discontinuous pine sites. A time-series of data from the discontinuous site during two partly cloudy days in February (days 50 and 51), one very clear day in March (day 84), and one overcast day in March (day 85) in 2003 show the extreme temporal variability of solar receipt at this

forested site (Fig. 4). The extinction of solar irradiance through the canopy is evident by the curve of the mean sub-canopy irradiance and the sunflecks of the individual pyranometers. For these 4 days, total irradiance measured at the forest floor varied from 17.1 (PSP2) to 49.7 MJ m⁻² (PSP7) as compared to 65.3 MJ m⁻² above the canopy. The measured solar transmissivity through the discontinuous canopy for this period ranged from 26 to 76%. In contrast, in the uniform, denser canopy, total irradiance at the forest floor for the same 4 days only varied from 15.1 to 21.1 MJ m⁻², and solar transmission ranged from 23 to 32%. During the partly cloudy and clear days, the total radiation occasionally reached the above canopy values because of canopy gaps. While during these same days, the sub-canopy diffuse radiation curve is approximated by the gray stippled curve that defines the overall minimum total radiation (rarely >100 W m⁻²) (Fig. 4). On the overcast day (day 85), radiation is primarily diffuse and tracks the above canopy curve at all pyranometer locations. Lacking above-canopy diffuse radiation, we are unable to measure transmissivity of the diffuse component and therefore we focus this analysis on total solar transmissivity.

3.2. Hemispherical photography and GLA analysis

A total of 38 hemispheric images were analyzed using the GLA software (10 from each of two forested sites over 2 years—two images were of poor quality). GLA output included predicted canopy openness, canopy LAI, and transmitted direct, diffuse, and total irradiance. The primary result of interest from the GLA software analysis was the predicted total solar transmissivity for the 6-day periods in February and the 6-day periods in March. Separate output was generated for the February and March periods.

3.3. Solar transmissivity

As an example of the results of the GLA analysis and transmission determination, GLA-predicted solar transmissivities were applied to the above-canopy irradiance (Eq. (3)) for the 10 pyranometer locations in the discontinuous pine forest (Fig. 5). As with the measured sub-canopy solar irradiance, the figure examines the same 4 days during 2003. The February transmission factors at each pyranometer location

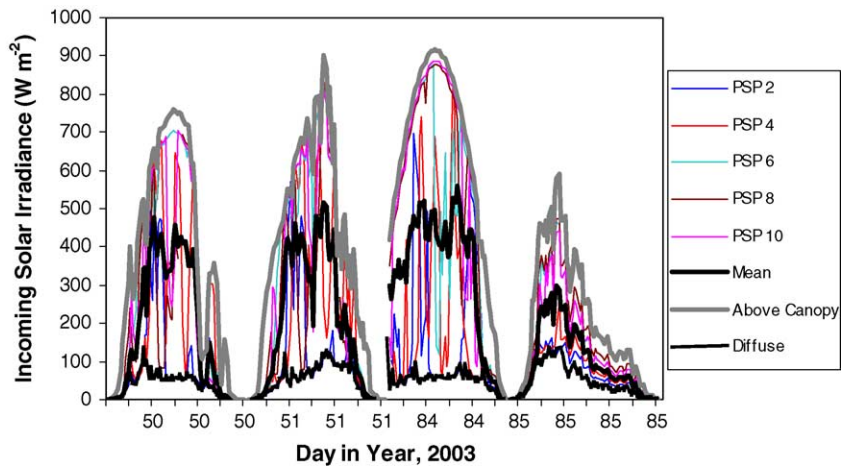


Fig. 4. Incoming solar irradiance measured beneath the discontinuous pine canopy showing data from five of the ten individual pyranometers, the mean of those data (thick black line), the above canopy irradiance (thick gray line) and the sub-canopy diffuse radiation (stippled line). Data are from 2 days in February and 2 days in March 2003.

were applied for days 50 and 51, while the March transmission factors were applied for days 84 and 85. In contrast to the measured data, the predicted sub-canopy irradiance curves are the same shape as the above-canopy data. This approach of using single transmittances does not replicate the sunfleck behavior but has strength in its simplicity (GLA software separately computes the sunfleck duration-frequency distribution). For these 4 days, the total predicted

irradiance at the forest floor varied from 18.0 MJ m^{-2} (PSP2 location) to 50.3 MJ m^{-2} (PSP7 location), which is less than 1 MJ m^{-2} higher than the measured data. In the uniform, denser canopy (data not shown), total predicted irradiance at the forest floor for the same 4 days varied from 17.0 to 20.6 MJ m^{-2} , within 2 MJ m^{-2} of measured.

Fig. 6 compares the curves of the mean measured and mean GLA-predicted irradiance from Figs. 4 and

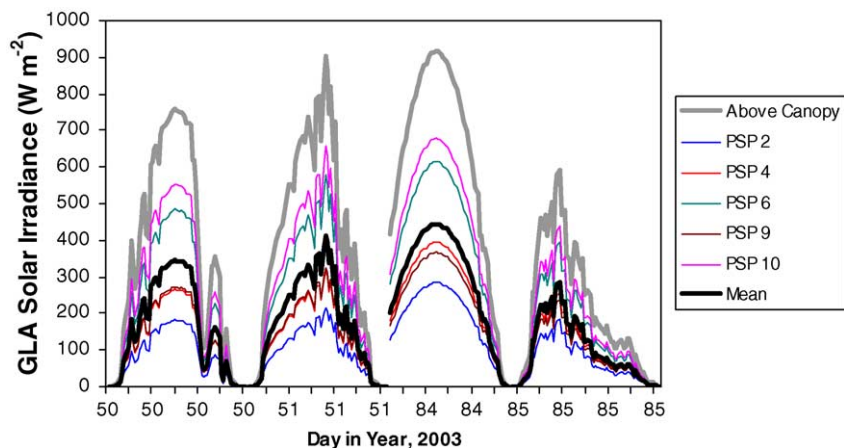


Fig. 5. GLA-predicted solar irradiance at 5 of the 10 sub-canopy pyranometer locations in the discontinuous pine canopy. The mean of those data (thick black line), and the above canopy irradiance (thick gray line) are presented. Predictions are for the same 2 days in February and 2 days in March 2003.

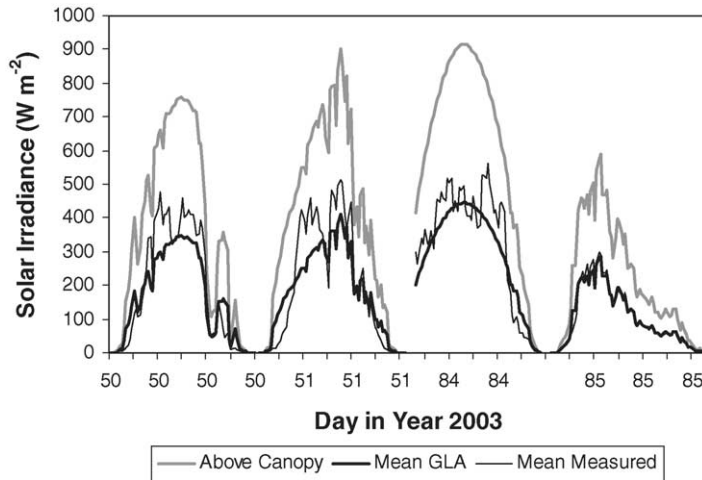


Fig. 6. Comparison of mean measured (thin black line) and GLA-predicted (thick black line) sub-canopy solar irradiance in the discontinuous pine canopy for 2003. The above canopy data are also shown (thick gray line).

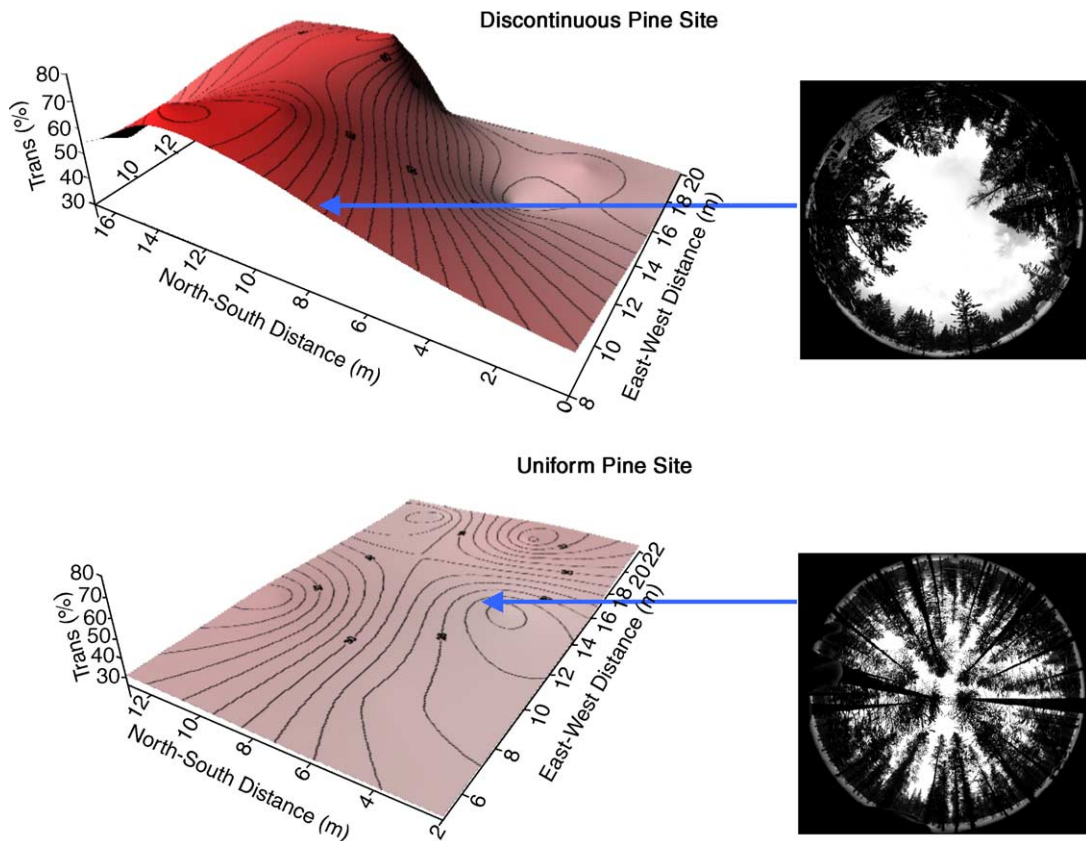


Fig. 7. Three-dimensional view with contours of mean daily solar transmissivity measured at each pyranometer location in March 2003 along with an example hemispheric photo. The darker shading represents higher transmissivities. The transmissivity contour intervals are 2% for the discontinuous site and 0.5% for the uniform site.

5 with the above-canopy irradiance. During the partly cloudy and clear days, the GLA software slightly over-predicted transmissivity at high solar zenith angles (early morning and evening) and under-predicted transmissivity at the low solar zenith angles (mid-day). In this case, an average GLA-determined transmittance cannot represent the extremes caused by different solar paths in the morning and evening and those at mid-day. The high zenith angle over-prediction is ascribable to the method of applying GLA-predicted transmission factors to above-canopy data. Multiplying the transmission factor determined from each radiometer by the measured above-canopy total irradiance data simply reduces the above-canopy data by a certain percentage. This technique cannot account for path lengths, sunflecks, and tree geometry; rather, it provides information on the mean estimated sub-canopy irradiance for the day. On the cloudy day, when the solar radiation is largely diffuse, the GLA software accurately predicted the sub-canopy irradiance.

A three-dimensional perspective on the spatial variability of measured solar transmissivities is presented in Fig. 7. Here, the mean daily solar transmissivity measured by each pyranometer in March 2003 is plotted for both forested sites along with an example hemispheric photo. The darker shading and greater relief represent higher transmissivities. The transmissivity contour intervals are 2% for the discontinuous site and 0.5% for the uniform site and show the high variability of transmissivity in the discontinuous site. Similarly, Rowlands et al. (2002) work at the same forested sites in Colorado, supports these observations of large variability of solar irradiance beneath the discontinuous site and the relatively small variability beneath the uniform canopy.

Considering all data from both the uniform and discontinuous canopies during 2002 and 2003, we find a good agreement between measured and GLA-predicted transmissivities. Fig. 8 shows the mean and standard deviations for all data collected in February of both years, in March of both years, and the 2 months combined. In all but one case, GLA over-predicted solar transmissivity, but given the error bars, this is insignificant. A scatterplot comparing measured versus GLA-predicted transmissivities from all 74 data points shows a strong relationship between the

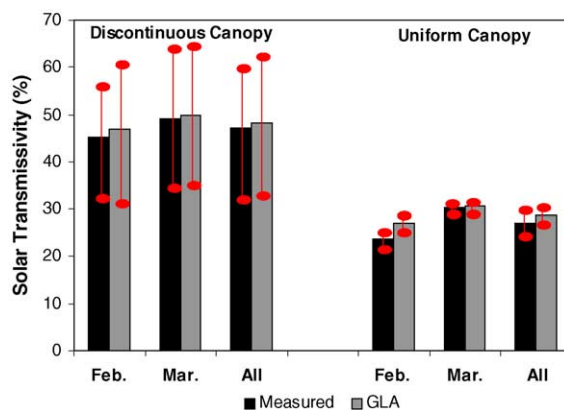


Fig. 8. Mean measured and GLA-predicted solar transmissivities for the February and March periods of both years considered separately and combined. Vertical lines show one standard deviation from the mean.

variables ($y = 0.95x + 3.32$; $r^2 = 0.86$), further supporting the use of hemispherical images with GLA software to determine sub-canopy solar transmission coefficients (Fig. 9).

The slight over-prediction of solar transmissivity by the GLA software may result because the camera was mounted approximately 1 m above the pyranometer, effectively reducing the tree height by 1 m. A comparison of film-based hemispherical images and digital based images by Frazer et al. (2001) showed

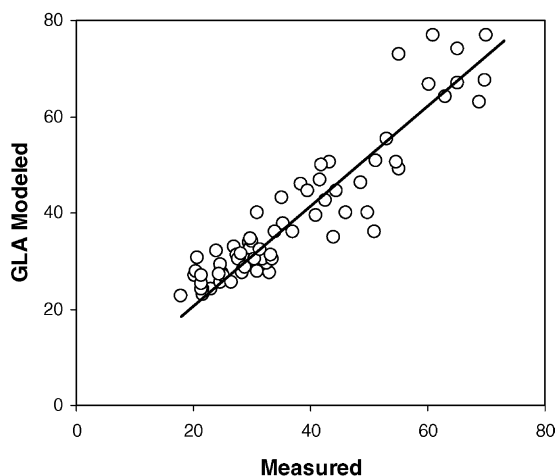


Fig. 9. Scatterplot and linear best-fit (least squares) for comparison of measured solar transmissivity with GLA-predicted solar transmissivity in percent ($y = 0.95x + 3.32$; $r^2 = 0.86$; $n = 74$).

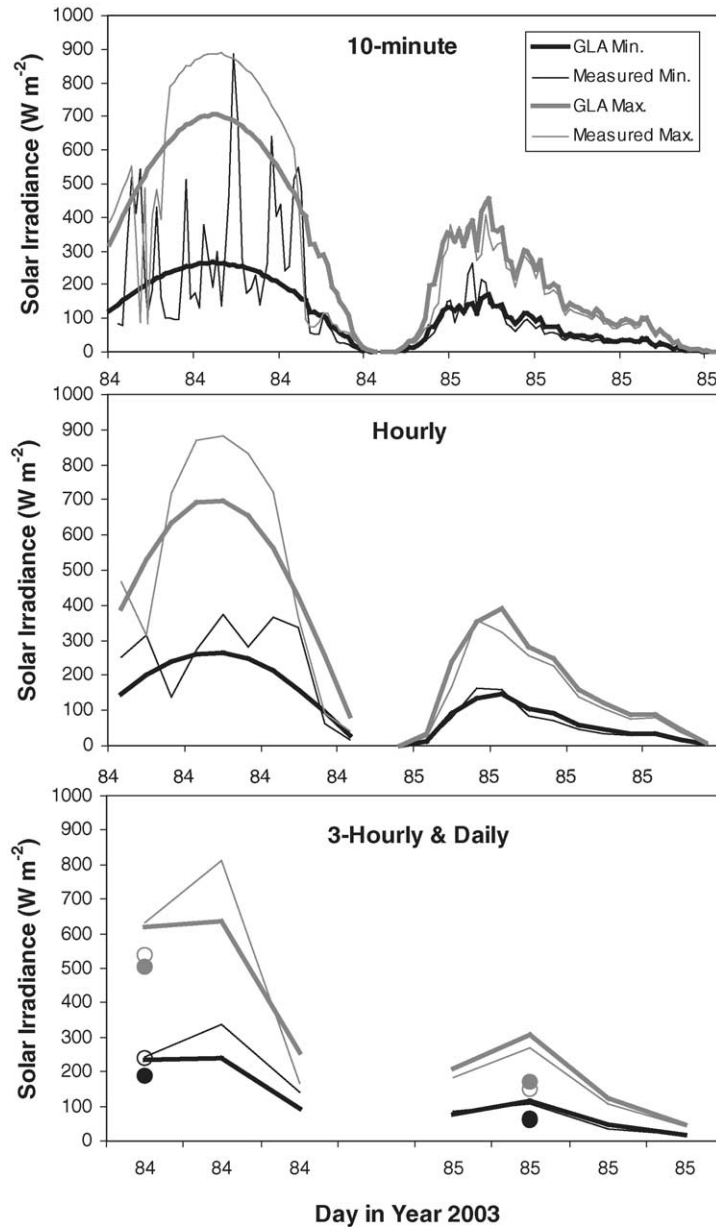


Fig. 10. Solar irradiance beneath the discontinuous pine site for a variety of time steps: (a) 10 min, (b) hourly, (c) 3-hourly, and daily. The thin lines and open circles represent measured data, and the thick lines and closed circles represent GLA-predicted values. The gray lines and circles correspond to PSP data or locations with highest transmissivities while black lines and circles correspond to data or locations with the lowest transmissivities.

that the Nikon Coolpix 950 with fisheye converter (a similar digital set-up to the one used in this study) produced canopy openness measures that were 1.4 times greater than the film estimates. As total solar

transmissivity is closely related to canopy openness, this may help explain the higher GLA-predicted transmissivities. Additionally, while GLA estimates of solar transmittance are determined from visible

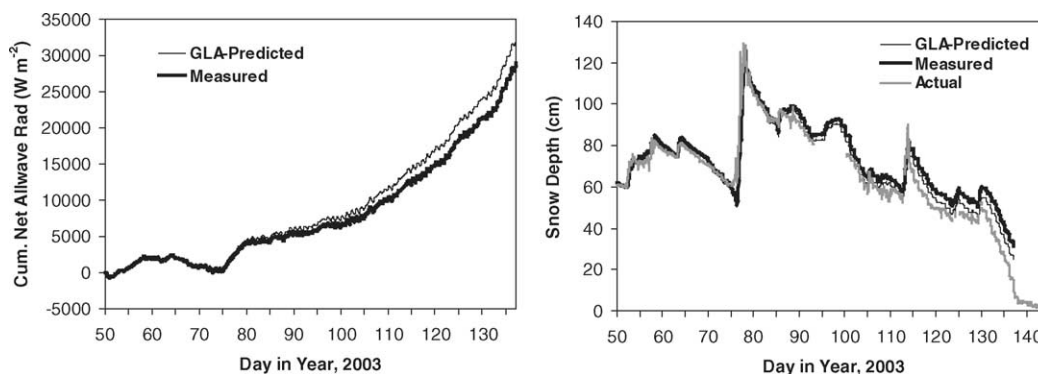


Fig. 11. The thick black lines show model results from applying the 2003 mean *measured* transmissivity (25.4%) to the above canopy solar data and driving the model with the resulting transmitted radiation. These results are compared to using a mean *GLA-predicted* transmissivity (27.9%) in the same way (thin black lines). Results are compared for cumulative net allwave radiation (a) and snow depth (b).

(0.36–0.75 μm) gaps, they are not completely comparable to measured transmissivities using the Eppley pyranometer that includes the near-IR wavelengths.

Finally, we look closely at the effect of the time step on the relationship between measured solar irradiance and predicted irradiance using GLA-determined transmission factors (Fig. 10). Data are presented for one clear day (day 84) and one cloudy day (day 85) in March 2003 comparing solar irradiance at time resolutions of 10 min, hourly, 3-hourly, and daily. The 10 min and hourly data clearly show that small variations in the solar zenith angle can induce large variations in transmitted solar irradiance because of the canopy structure. The ideal time resolution depends on the application of transmissivity estimates. As noted by Percy et al. (1994), sunflecks can provide an important resource to plant photosynthesis, depending on the timescale. Percy (1990) found that sunflecks longer than 10 min may contribute more than two-thirds of the daily incoming radiation. For each application, there must be a range of optimum time resolutions; a finer time resolution would be noisy due to the local arrangement of branches, whereas a coarser time resolution would not allow detection of the crown effects (Roujean, 1999). For biological considerations, frequency and duration of sunflecks during the diurnal cycle are of significance. For modeling snowpack energy balance over a period of weeks or months, mean values of transmissivity may be adequate.

3.4. SNOBAL modeling

Snow modeling from mid-February through complete snow ablation in June 2003 shows the impact of using measured transmissivities versus GLA-predicted transmissivities (Fig. 11). The thick black lines show model results from applying the 2003 mean measured transmissivity (25.4%) to the above canopy solar data and driving the model with the resulting transmitted radiation. These results are compared to using a mean GLA-predicted transmissivity (27.9%) in the same way (thin black lines). In this modeling exercise, applying the GLA-predicted transmissivity to above-canopy solar data for driving SNOBAL improved snow depth predictions compared to applying the measured transmissivities.

4. Conclusions

Incoming solar radiation under canopies has a high degree of both temporal and spatial variability as observed from our pyranometer array data beneath uniform and discontinuous pine canopies. The use of hemispherical photography captures the geometry of the canopy and, along with GLA analysis software, provides an inexpensive and simple means of obtaining good solar transmissivity estimates for periods of interest. On clear sky days, GLA overestimates irradiance at low sun angles and under-

estimates irradiance at high sun angles. On cloudy days (e.g., day 85), GLA estimates diffuse light very well. GLA-predicted solar transmittance through canopies provided good estimates for many applications, including snow ablation modeling and analysis of sub-canopy fluxes. For some applications, such as a forest with uniform canopy properties, using hemispherical images and analysis software to determine transmission of solar radiation through a canopy may negate the need for full radiometer arrays. High quality pyranometers are expensive and sub-canopy solar variability requires the use of multiple radiometers. In northern latitudes, multiple deployments of arrays are required to address issues pertaining to sun angle positions. Also, the in-field maintenance of radiometers, especially during winter months, is considerable. Any number of hemispherical images can be taken to reduce the uncertainty attributable to variability and the images remain valid as long as the growth of the trees is minimal. Additionally, one image can be used to predict transmissivity during all seasons, as the software calculates sun angles based on location and time of year. Future work will include efforts to distribute this method over complex, sloped terrain and to determine transmission factors from the GLA software for shorter time steps (i.e., hourly). Additionally, we will evaluate hemispherical photography for use in determining longwave transmission through discontinuous canopies.

Acknowledgements

This work was funded through cooperation of the National Aeronautics and Space Administration (NASA) and the US Army Basic Research Program. The authors gratefully acknowledge efforts of D. Cline, K. Elder, G. Goodbody, T. Graf, R. Davis, and M. Martinez in support of this research. We also acknowledge two anonymous reviewers for providing constructive comments that improved this manuscript.

References

- Anderson, M.C., 1964. Studies of the woodland light climate. I. The photographic computation of light conditions. *J. Ecol.* 52, 27–41.
- Canham, C.D., 1988. An index for understory light levels in and around canopy gaps. *Ecology* 69 (5), 1634–1638.
- Canham, C.D., 1995. GLI/C: Software for Calculation of Light Transmission through Forest Canopies Using Color Fisheye Photography. Institute of Ecosystem Studies, Millbrook, NY, USA.
- Chen, J.M., Black, T.A., Adams, R., 1991. Evaluation of hemispherical photography for determining plant area index and geometry of a forest stand. *Agric. For. Meteorol.* 56, 129–143.
- Cline, D., Elder, K., Davis, R., Hardy, J., Liston, G., Imel, D., Yueh, S., Gasiewski, A., Koh, G., Armstrong, R., Parsons, M., 2002. Overview of the NASA Cold Land Process Field Experiment. Microwave Remote Sensing of the Atmosphere and Environment III, Proceedings of the SPIE, vol. 4894. Hangzhou, China, 24–25 October, pp. 361–372.
- Evans, G.C., Coombe, D.E., 1959. Hemispherical and woodland canopy photography and the light climate. *J. Ecol.* 47, 103–113.
- Frazer, G.W., Canham, C.D., Lertzman, K.P., 1999. Gap Light Analyzer (GLA), Version 2.0: Imaging Software to Extract Canopy Structure and Gap Light Transmission Indices from True-color Fisheye Photographs, Users Manual and Program Documentation. Copyright 1999: Simon Fraser University/Institute of Ecosystem Studies, Burnaby, BC/ Millbrook/NY.
- Frazer, G.W., Canham, C.D., Lertzman, K.P., 2000. Gap Light Analyzer (GLA), Version 2.0. Technological Tools. *Bulletin of the Ecological Society of America*, pp. 191–197.
- Frazer, G.W., Fournier, R.A., Trofymow, J.A., Hall, R.J., 2001. A comparison of digital and film fisheye photography for analysis of forest canopy structure and gap light transmission. *Agric. For. Meteorol.* 109, 249–263.
- Frew, J.E., 1990. The image processing workbench. PhD Dissertation. University of California, Santa Barbara.
- Gendron, F., Messier, C., Comeau, P.G., 1998. Comparison of various methods for estimating the mean growing season percent photosynthetic photon flux density in forests. *Agric. For. Meteorol.* 92, 55–70.
- Hardy, J.P., Davis, R.E., Jordan, R., Li, X., Woodcock, C., Ni, W., McKenzie, J.C., 1997. Snow ablation modeling at the stand scale in a boreal jack pine forest. *J. Geophys. Res.* 102 (N24), 29397–29406.
- Hardy, J.P., Davis, R.E., Jordan, R., Ni, W., Woodcock, C., 1998. Snow ablation modelling in a mature aspen stand of the boreal forest. *Hydrol. Process.* 12 (10/11), 1763–1778.
- Hardy, J.P., Groffman, P.M., Fitzhugh, R.D., Henry, K.S., Welman, T.A., Demers, J.D., Fahey, T.J., Driscoll, C.T., Tierney, G.L., Nolan, S., 2001. Snow depth manipulation and its influence on soil frost and water dynamics in a northern hardwood forest. *Biogeochemistry* 56 (2), 151–174.
- Hellstrom, R., 2000. Forest cover algorithms for estimating meteorological forcing in a numerical snow model. *Hydrol. Process.* 14, 3239–3256.
- Li, X., Strahler, A., Woodcock, C., 1995. A hybrid geometric optical-radiative transfer approach for modelling albedo and directional reflectance of discontinuous canopies. *IEEE Trans. Geosci. Remote Sensing* 33 (2), 466–480.
- Lin, T.-C., Chiang, J.-M., 2002. Applications of hemispherical photographs in studies of forest ecology. *Taiwan J. For. Sci.* 17 (3), 387–400 (in Chinese with English summary).

- Link, T., Marks, D., 1999. Distributed simulation of snowcover mass- and energy-balance in the boreal forest. *Hydrol. Process.* 13 (14/15), 2439–2452.
- Link, T., Marks, D., Hardy, J., in press. A deterministic method to characterize canopy radiative transfer properties. *Hydro. Process.*
- Marks, D., 1988. Climate, energy exchange, and snowmelt in Emerald Lake watershed, Sierra Nevada. Ph.D. Dissertation. Departments of Geography and Mechanical Engineering, University of California, Santa Barbara, p. 158.
- Marks, D., Domingo, J., Frew, J., 1999. Software tools for hydroclimatic modeling and analysis: Image Processing Workbench, ARS – USGS, Version 2, ARS Technical Bulletin 99-1. Northwest Watershed Research Center, USDA Agricultural Research Service, Boise, ID. <http://www.nwrc.ars.usda.gov/ipw>.
- Melloh, R., Hardy, J., Bailey, R., Hall, T., 2002. An efficient snow albedo model for the open and sub-canopy. *Hydrol. Process.* 16 (18), 3571–3584.
- Nakabayashi, H., Ishikawa, N., Kodama, Y., 1999. Radiative characteristics in a Japanese forested drainage basin during snowmelt. *Hydrol. Process.* 13, 157–167.
- Ni, W., Li, X., Woodcock, C., Roujean, J.-L., Davis, R.E., 1997. Transmission of solar radiation in boreal conifer forests: measurements and models. *J. Geophys. Res.* 102 (N24), 29555–29566.
- Nijssen, B., Lettenmaier, D.P., 1999. A simplified approach for predicting shortwave radiation transfer through boreal forest canopies. *J. Geophys. Res.* 104, 27859–27868.
- Pearcy, R.W., 1990. Sunflecks and photosynthesis in plant canopies. *Ann. Rev. Plant Physiol. Plant Mol. Biol.* 41, 421–453.
- Pearcy, R.W., Chazdon, R.I., Gross, L.J., Mott, K.A., 1994. Photosynthetic utilization of sunflecks: a temporally patchy resource on a timescale of seconds to minutes. In: Caldwell, M.M., Pearcy, R.W. (Eds.), *Exploitation of Environmental Heterogeneity by Plants-Ecophysiological Process Above- and-Belowground*. Academic Press, San Diego, CA, pp. 175–208.
- Pomeroy, J.W., Dion, K., 1996. Winter radiation extinction and reflection in a boreal pine canopy: measurements and modelling. *Hydrol. Process.* 10, 1591–1608.
- Rich, P., 1990. Characterizing plant canopies with hemispherical photographs. *Remote Sensing Rev.* 5 (1), 13–29.
- Roujean, J.-L., 1999. Two-story equations of transmission of solar energy (TSETSE) in open boreal conifer tree stands. *J. Geophys. Res.* 104 (D22), 27869–27879.
- Rowlands, A.P., Pomeroy, J.W., Hardy, J.P., Marks, D., Elder, K., Melloh, R., 2002. Small-scale variability of radiant energy for snowmelt in a mid-latitude sub-alpine forest. In: *Proceedings of the Eastern Snow Conference*, vol. 59, pp. 93–108.
- Tarboton, D., Luce, C., 1996. Utah energy balance snow accumulation and melt model (UEB), computer model technical descriptions and users guide. Utah Water Research Laboratory, Utah State University and USDA Forest Service, Intermountain Research Station.
- Tribbeck, M., 2002. Modelling the effect of vegetation on the seasonal snow cover. PhD Thesis. University of Reading, UK.
- Whitford, K.R., Colquhoun, L.J., Land, A., Harper, B., 1995. Measuring leaf area index in a sparse eucalypt forest: a comparison of estimates from direct measurements, hemispherical photography, sunlight transmittance and allometric regression. *Agric. For. Meteorol.* 74:, 237–249.
- Wigmosta, M., Vail, L., Lettenmaier, D., 1994. A distributed hydrology-vegetation model for complex terrain. *Water Resour. Res.* 30 (6), 1665–1679.